Physics-based Edge Evaluation for Improved Color Constancy

Arjan Gijsenij[1], Theo Gevers[1] and Joost van de Weijer[2]
[1] Intelligent Systems Lab Amsterdam
University of Amsterdam
Science Park 107, 1098 XG Amsterdam
{a.gijsenij,th.gevers}@uva.nl

[2] Computer Vision Center
Campus Universitat Autònoma de Barcelona
08193 Bellaterra, Barcelona
joost@cvc.uab.es

Abstract

Edge-based color constancy makes use of image derivatives to estimate the illuminant. However, different edge types exist in real-world images such as shadow, geometry, material and highlight edges. These different edge types may have a distinctive influence on the performance of the illuminant estimation.

Therefore, in this paper, an extensive analysis is provided of different edge types on the performance of edge-based color constancy methods. First, an edge-based taxonomy is presented classifying edge types based on their reflectance properties (e.g. material, shadow-geometry and highlights). Then, a performance evaluation of edge-based color constancy is provided using these different edge types. From this performance evaluation, it is derived that certain edge types are more valuable than material edges for the estimation of the illuminant. To this end, the weighted Grey-Edge algorithm is proposed in which certain valuable edge types are more emphasized for the estimation of the illuminant.

From the experimental results, it is shown that the proposed weighted Grey-Edge algorithm based on the shadow-shading variant, i.e. assigning higher weights to edges with more energy in the shadow-shading direction, results in the best performance. Moreover, all current state-of-the-art methods, including pixel-based methods and edge-based methods, have been significantly outperformed by the proposed weighted Grey-Edge algorithm, resulting in an improvement of 9% *over the current best-performing algorithm.*

1. Introduction

Changes in illumination cause the measurements of object colors to be biased towards the color of the light source. Color constancy is the ability to maintain invariance with respect to these changes. The ability of color constancy facilitates many computer vision related tasks like color feature extraction [17] and color appearance models [9].

Many computational color constancy algorithms have been proposed, see e.g. [20] for an overview. Traditionally, color constancy methods use pixel values of an image to estimate the illuminant. Examples of such methods include approaches based on low-level features [5, 14, 22] and gamut-based algorithms [11, 13, 15]. Only recently, methods that use derivatives (i.e. edges) and even higher-order statistics have been proposed [6, 7, 19, 24].

From earlier studies on pixel-based color constancy, it is known that highlights (under the assumption of the neutral interface reflection) contain important information about the color of the light source [1, 3]. Other work shows that, using zeroth-order statistics, a varying illumination can aid the estimation of the illuminant, if surfaces are accurately identified under different light sources [2, 10, 25]. However, prior knowledge about the scene is required to classify pixels into e.g. material and highlight pixels reducing the applicability of the methods [1, 2, 3, 10]. Therefore, in this paper, the focus will be on edge-based color constancy.

Various edge classification schemes have been proposed which categorize edges based on their reflectance characteristics and physical nature [12, 16, 18, 23]. For example, edges can be classified into material edges (e.g. edges between objects), shadow/shading edges (e.g. edges caused by the geometry of an object) and specular edges (e.g. highlights). Edge-based color constancy makes use of image derivatives to estimate the illuminant, and consequently, different edge types may provide a different impact on the performance of the illuminant estimation. Although, edge-based color constancy show promising results, an analysis of different edge types has not been studied.

Therefore, in this paper, an extensive analysis is provided of the physical nature of different edge types on the performance of edge-based color constancy methods. Further, a weighted Grey-Edge algorithm is proposed to improve edge-based color constancy. To this end, first, an edge-based taxonomy is presented classifying edge types based on their reflectance properties (e.g. material, shadow-

geometry and highlights). Then, a performance evaluation of edge-based color constancy is provided using these different edge types. From this performance evaluation, it is derived that certain edge types are more valuable than material edges for the estimation of the illuminant. To this end, the weighted Grey-Edge algorithm is proposed in which certain edge types are more emphasized than others for the estimation of the illuminant.

This paper is organized as follows. In section 2, color constancy is discussed, followed by a categorization of edges into several types in section 3. In section 4, the performance of edge-based color constancy is analyzed with respect to different edge types. Then, in section 5, the weighted Grey-Edge algorithm is proposed.

2. Color Constancy

The image values $\mathbf{f}$ for a Lambertian surface depend on the color of the light source $e(\lambda)$, the surface reflectance $s(\mathbf{x}, \lambda)$ and the camera sensitivity function $\mathbf{c}(\lambda)$:

$$\mathbf{f}(\mathbf{x}) = \int_{\omega} e(\lambda)\mathbf{c}(\lambda)s(\mathbf{x}, \lambda)d\lambda, \tag{1}$$

where ω is the visible spectrum, λ is the wavelength of the light and $\mathbf{x}$ is the spatial coordinate. Assuming that the scene is illuminated by one light source and that the observed color of the light source $\mathbf{e}$ depends on the color of the light source $e(\lambda)$ as well as the camera sensitivity function $\mathbf{c}(\lambda)$, then color constancy is equivalent to the estimation of $\mathbf{e} = \int_{\omega} e(\lambda)\mathbf{c}(\lambda)d\lambda$, given the image values of $\mathbf{f}$, since both $e(\lambda)$ and $\mathbf{c}(\lambda)$ are, in general, unknown. This is an under-constrained problem and therefore it can not be solved without further assumptions.

2.1. Pixel-based Color Constancy

Two well-known and often used algorithms are based on the Retinex Theory proposed by Land [22]. The White-Patch algorithm is based on the White-Patch assumption, i.e. the assumption that *the maximum response in the RGB-channels is caused by a white patch*. The second algorithm, the Grey-World algorithm [5] is based on the Grey-World assumption, i.e. *the average reflectance in a scene is achromatic*. Another type of algorithms are gamut-based methods, originally proposed by Forsyth [15]. Gamut-based algorithms use more advanced statistical information about the image, and are based on the assumption, that *in real-world images, one observes, under a given illuminant, only a limited number of different colors*. Even though the White-Patch, Grey-World and gamut mapping are completely different algorithms, they all have in common that they estimate the illuminant using only the pixel values in an image.

2.2. Edge-based Color Constancy

Recently, pixel-based methods are extended to incorporate derivative information (i.e. edges) and higher-order statistics, resulting in the Grey-Edge [24] and the derivative-based gamut mapping [19].

The Grey-Edge actually comprises a framework that incorporates zeroth-order methods (e.g. the Grey-World and the White-Patch algorithms), first-order methods (e.g. the Grey-Edge), as well as higher-order methods (e.g. 2^{nd}-order Grey-Edge). Many different algorithms can be created by varying the three parameters:

$$\left(\int \left| \frac{\partial^n \mathbf{f}_{\sigma}(\mathbf{x})}{\partial \mathbf{x}^n} \right|^p d\mathbf{x} \right)^{\frac{1}{p}} = k\mathbf{e}_{n,p,\sigma}, \tag{2}$$

where n is the order of the derivative, p is the Minkowski-norm and $\mathbf{f}^{\sigma}(\mathbf{x}) = \mathbf{f} \otimes \mathbf{G}^{\sigma}$ is the convolution of the image with a Gaussian filter with scale parameter σ. Good results are obtained by using instantiation $e_{1,1,\sigma}$, i.e. a simple average of the edges at scale σ also called the Grey-Edge method [24].

Another extension of pixel-based methods to incorporate derivative information involves the gamut mapping. This method has been extended to include not only pixel values, but also linear combinations of pixel values, e.g. image derivatives. The use of image derivatives has some advantages over using pixel values directly as certain effects that cause a failure of the diagonal model, like scattered light, have little effects on the derivative of an image. It is shown that the derivative-based gamut mapping suffers less from these degrading conditions [19]. Therefore, in addition to the Grey-Edge method, the derivative-based gamut mapping method is used as a different type of color constancy method to assess the influence of different edge types.

3. Photometric Edge Types

Edges can be categorized into several types based on their reflectance such as material edges, shadow/shading edges and specular edges [12, 16, 18, 23]. Material edges are edges between two different surfaces or objects. Shading edges are edges that are caused by the geometry of an object, for instance by a change in surface orientation with respect to the illumination. Shadow edges are cast shadows, caused by an object that (partially) blocks the light source. Specular edges are edges that are caused by highlights. Besides these main edge types, several other types exists. However, two derivations will be discussed and analyzed in this paper.

First, a shadow edge can be either a sudden change of intensity, e.g. caused by the geometry of an object, or it can be somewhat differently colored. When the latter is the case, then the sudden gradient is not only an intensity gradient but it also contains a faint color gradient at the same

time. Hence, a shadow edge can be divided into an intensity shadow edge and a colored shadow edge. When we refer to shadow edges in general, the union of these two edge types is implied. Furthermore, in real-world images, interreflection is an important aspect. Interreflection is the effect of light reflected from one surface onto a second surface. This effect changes the overall illumination that is received by the second surface, and hence the color of this surface. In this paper, interreflection edges are the fifth edge type that is analyzed.

3.1. Reflectance-based Edge Classification

Classification of edges into different types can be done using a set of photometric variants and quasi-invariants [23]. To this end, the derivative of an image, $\mathbf{f}_x = (R_x, G_x, B_x)^T$, is projected on three directions called *variant directions*. By removing the variance from the derivative of the image, a complementary set of derivatives is constructed called *quasi-invariants*.

The projection of the derivative on the shadow-shading direction is called the shadow-shading variant and is defined as:

$$\mathbf{S}_x = \left(\mathbf{f}_x \cdot \hat{\mathbf{f}}\right) \hat{\mathbf{f}}, \tag{3}$$

where $\hat{\mathbf{f}} = \frac{1}{\sqrt{R^2+G^2+B^2}}(R, G, B)^T$ indicates the direction of the variant and the dot indicates the vector inner product. The shadow-shading variant is that part of the derivative which could be caused by shadow or shading. What remains after subtraction of the variant from the derivative is called the shadow-shading quasi-invariant:

$$\mathbf{S}_x^c = \mathbf{f}_x - \mathbf{S}_x. \tag{4}$$

The quasi-invariant $\mathbf{S}_x^c$ is insensitive to shadow-shading edges, hence contains only specular and material edges.

Using the same reasoning, a specular variant and quasi-invariant is obtained:

$$\mathbf{O}_x = \left(\mathbf{f}_x \cdot \hat{\mathbf{c}}^i\right) \hat{\mathbf{c}}^i, \tag{5}$$

$$\mathbf{O}_x^c = \mathbf{f}_x - \mathbf{O}_x, \tag{6}$$

where $\hat{\mathbf{c}}^i$ is the specular direction. The specular quasi-invariant is insensitive to highlight edges.

Finally, the shadow-shading-specular variant and quasi-invariant can be constructed by projecting the derivative on the hue direction:

$$\mathbf{H}_x = \left(\mathbf{f}_x \cdot \hat{\mathbf{b}}\right) \hat{\mathbf{b}}, \tag{7}$$

$$\mathbf{H}_x^c = \mathbf{f}_x - \mathbf{H}_x, \tag{8}$$

where $\hat{\mathbf{b}}$ is the hue direction. $\mathbf{H}_x^c$ does not contain specular or shadow-shading edges.

These quasi-invariants can be used for edge classification [23]. If little of the energy of an edge is directed towards the shadow-shading-specular direction, then this edge is classified as a material edge. An edge is classified as shadow edge if more energy is directed towards the shadow-shading direction than towards the specular direction. Finally, if more energy is in the specular direction than in the shadow-shading direction, then this edge is classified as specular edge.

4. Performance using Different Edge Types

In this section, the aim is to analyze which edge types have the most influence on the accuracy of the illuminant estimation. To this end, a spectral data set is used first to generate different edges types under controlled circumstances. On this data set, the two different edge-based color constancy algorithms are evaluated i.e. the Grey-Edge and the derivative-based gamut mapping approach . Then, the quasi-invariants are used to classify edges in real-world images into material and shadow edges, extending the experiments from a controlled setting to real-world scenarios.

To evaluate the performance of color constancy algorithms, the angular error ϵ is widely used [21]. This measure is defined as the angular distance between the actual color of the light source $\mathbf{e}_l$ and the estimated color $\mathbf{e}_e$:

$$\epsilon = \cos^{-1}(\hat{\mathbf{e}}_l \cdot \hat{\mathbf{e}}_e), \tag{9}$$

where $\hat{\mathbf{e}}_l \cdot \hat{\mathbf{e}}_e$ is the dot product of the two normalized vectors representing the true color of the light source $\mathbf{e}_l$ and the estimated color of the light source $\mathbf{e}_e$. To measure the performance of an algorithm on a whole data set, the median angular error is reported.

4.1. Spectral data

The first experiments are performed using the spectral data set introduced by Barnard et al. [4]. This set consists of 1995 surface reflectance spectra and 287 illuminant spectra, from which an extensive range of surfaces (i.e. RGB-values) can be generated using eq. (1). For these experiments, the following types of surfaces are created:

- Material surface $\mathbf{m}_i$:

$$\mathbf{m}_{ik} = \int_\omega e_k(\lambda)\mathbf{c}(\lambda)s_i(\mathbf{x}, \lambda)d\lambda. \tag{10}$$

- Intensity shadow surface $\mathbf{p}_i$:

$$\mathbf{p}_{ik} = \int_\omega \frac{e_k(\lambda)}{\phi}\mathbf{c}(\lambda)s_i(\mathbf{x}, \lambda)d\lambda. \tag{11}$$

- Colored shadow surface $\mathbf{q}_i$:

$$\mathbf{q}_{ikk'} = \mathbf{p}_{ik} + \eta \int_\omega e_{k'}(\lambda)\mathbf{c}(\lambda)s_i(\mathbf{x}, \lambda)d\lambda, \tag{12}$$

- Specular surface $\mathbf{h}_{ik}$:

$$\mathbf{h}_{ik} = \mathbf{m}_{ik} + \gamma \int_\omega e_k(\lambda)\mathbf{c}(\lambda)d\lambda, \tag{13}$$

- Interreflection surface $\mathbf{r}_{ijk}$:

$$\mathbf{r}_{ijk} = \mathbf{m}_{jk} + \theta \mathbf{m}_{ik}, \tag{14}$$

where the subscript i and j denote different surface reflectance spectra and k and k' denote different illuminant spectra. Furher, ϕ and γ are random variables uniformly distributed between 1 and 4, and η and θ are random variables uniformly distributed between 0 and 0.25.

Since the focus is on edge-based color constancy, the following transitions (i.e. edges) between surfaces are generated:

- Material edge: $\mathbf{m}_{ik} - \mathbf{m}_{jk}$.
- Intensity shadow edge: $\mathbf{m}_{ik} - \mathbf{p}_{ik}$.
- Colored shadow edge: $\mathbf{m}_{ik} - \mathbf{q}_{ikk'}$.
- Specular edge: $\mathbf{m}_{ik} - \mathbf{h}_{ik}$.
- Interreflection edge: $\mathbf{m}_{ik} - \mathbf{r}_{ijk}$.

Note that these edges can be considered to be step edges. In real-world scenes, transitions are likely to be more gradual. However, for the purpose of this analysis, these edges are used to give a best-case assessment of algorithm performance.

4.2. Different number of edges

In the first experiment, the performance of two edge-based color constancy algorithms is analyzed with respect to different edge types. Using the spectral data set, a number of random surfaces are created, including n material surfaces, n intensity shadow surfaces, n colored shadow surfaces, n specular surfaces and n interreflection surfaces, resulting in a total of $5n$ surfaces. Note that to create these surfaces, the same illuminant is used. Using these surfaces, n material edges, n intensity shadow edges, n colored shadow edges, n specular edges and n interreflection edges are created. Two edge-based color constancy algorithms are evaluated (the Grey-Edge algorithm and the Derivative-based gamut mapping) by gradually increasing the number of edges. For each value of n ($n = \{4, 8, 16, 32, 64, 128, 256, 512, 1024\}$), the experiment is repeated 1000 times.

In figure 1(a), the median angular error for the Grey-Edge algorithm is shown differentiated by the five edge types. Remarkably, the angular error when using intensity shadow edges is significantly lower than when using material edges. As expected, color constancy based on specular edges results in a close to ideal performance. Further, the performance using the colored shadow edges and the interreflection edges is similar to the performance when using the material edges. The performance of the Derivative-based gamut mapping, see figure 1(b), shows a similar trend. Using specular edges results in near-perfect color constancy, and intensity shadow edges are more favorable than the other types of edges.

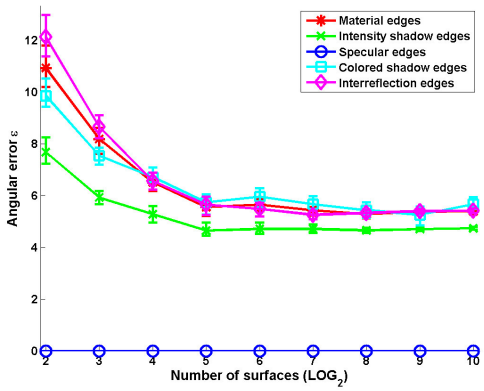

(a) Grey-Edge

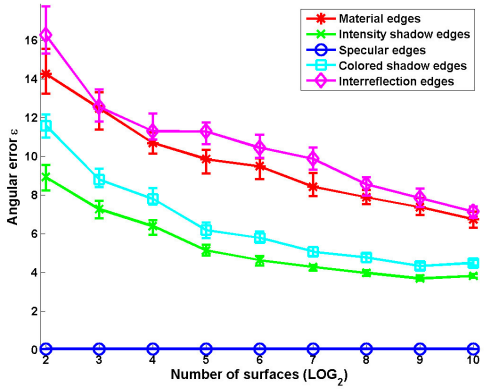

(b) Derivative-based Gamut mapping

Figure 1. Median angular error of the Grey-Edge, figure (a), and the Derivative-based Gamut mapping, figure (b), including a 95% confidence interval, using several different edge types.

4.3. Gamuts of different edge types

To study the observation why using shadow edges results in a better performance than when using material and other types of edges, the distribution of different edge types is considered. For the ease of illustration of the physical properties of edge types, the edges are converted to the opponent color space:

$$O1_x = \frac{R_x - G_x}{\sqrt{2}}, \tag{15}$$

$$O2_x = \frac{R_x + G_x - 2B_x}{\sqrt{6}}, \tag{16}$$

$$O3_x = \frac{R_x + G_x + B_x}{\sqrt{3}} \tag{17}$$

where R_x, G_x and B_x are derivatives of the R, G and B channels, respectively.

The distribution of edges in opponent color space is shown in figure 2. From these graphs, it can be derived that the variation in edge color is much higher for the material edges, figure 2(a), than for shadow edges, figures 2(b) and (c). Further, the intensity shadow edges are more di-

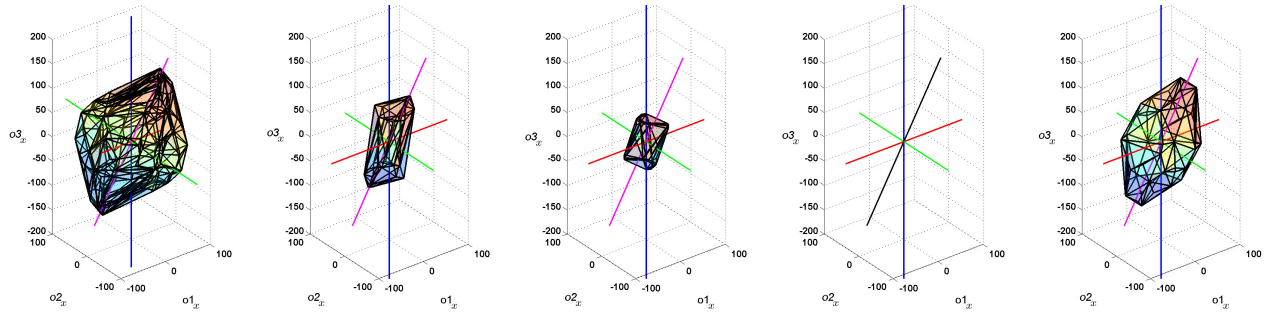

(a) (b) (c) (d) (e)

Figure 2. Gamut in opponent color space of several edge types put under one illuminant which is specified by the fourth axis. Shown are material edges in figure (a); intensity shadow edges in figure (b); colored shadow edges in figure (c); specular edges in figure (d); interreflection edges in figure (e).

rected towards the color of the light source (shown by the fourth axis) than the colored shadow edges. The shape of the gamut of the color shadow edges, which appears to be less directed towards the color of the light source than other edge types, can be explained by the influence of the second light source. The gamut of interreflection edges, figure 2(e), is similar to the material edges. Finally, specular edges, figure 2(d), all align perfectly with the color of the light source (shown by the fourth axis).

These graphs show that it is beneficial to use edges that are aligned with the color of the light source. The specular edges are all distributed on the diagonal representing the color of the light source, and near-perfect color constancy can be obtained using these edges. This observation is in accordance to pixel-based highlight analysis, where highlights contain valuable information about the color of the light source [1, 3]. Shadow edges are distributed denser around the color of the light source than material edges and interreflection edges, resulting in a higher performance.

Color clipping. In practice, pixel values are often bound to a certain maximum value. This effect is called color clipping. Since the specular surfaces have the highest RGB-values, these surfaces (and consequently the specular edges) risk to be affected by color clipping. To analyze this effect, a second experiment is performed where the generated RGB-values are color clipped at a gradually decreasing value. The results of this experiment for the Grey-Edge algorithm are shown in figure 3. The Derivative-based gamut mapping reveals a similar trend (not shown here). It can be seen that the performance using the specular edges immediately starts to decrease significantly, while the performance of the material and the shadow edges is not affected until 40% of the pixels are color clipped. The effects of color clipping cause the gamuts of the specular edges to shift towards the intensity axis ($O3_x$), hence the estimate of the illuminant will be biased towards white. Color clipping is an often occurring phenomena and cannot be prevented in practice.

To conclude, from an analytical approach, it can be derived that using specular edges for edge-based color constancy results in a close to ideal performance, because the specular edges align with the color of the light source. However, in practice, color clipping eliminates the advantages of specular edges and causes a significant decrease in performance. Shadow edges contain more variation than specular edges but are still aligned with the color of the light source. Consequently, the performance of edge-based color constancy using shadow edges degrades slightly. However, as material edges vary even more, their performance degrades even more. Although, interreflection edges vary less than material edges, they are not aligned with the color of the light and hence their performance is the worst. Hence, shadow edges are the preferred type of edges for accurate color constancy.

5. Weighted Grey-Edge Algorithm

In the previous section, it was shown that using shadow edges results in a more accurate performance than material edges. Therefore, in this section, the weighted Grey-Edge algorithm is proposed based on physics principles. For now, assume the original edge-based framework of eq. (2) to be reduced to the first-order Grey-Edge with a Minkowski-norm of 1, leading to a simplified version of eq. (2):

$$\int |\mathbf{f}_{\mathbf{x}}(\mathbf{x})| d\mathbf{x} = k\mathbf{e}, \tag{18}$$

where $\mathbf{f}_{\mathbf{x}}(\mathbf{x})$ is the derivative of image $\mathbf{f}$ at a certain scale. Then, the weighted Grey-Edge algorithm is given by:

$$\int |w(\mathbf{f}_{\mathbf{x}})^{\kappa} \mathbf{f}_{\mathbf{x}}(\mathbf{x})| d\mathbf{x} = k\mathbf{e}, \tag{19}$$

where $w(\mathbf{f}_{\mathbf{x}})^{\kappa}$ is a weighting function that assigns a weight to every value of $\mathbf{f}_x$. The power κ can be used to enforce the differences between high weights and medium weights. For now, we take $\kappa = 1$. Alternative values can be used depending on the data set.

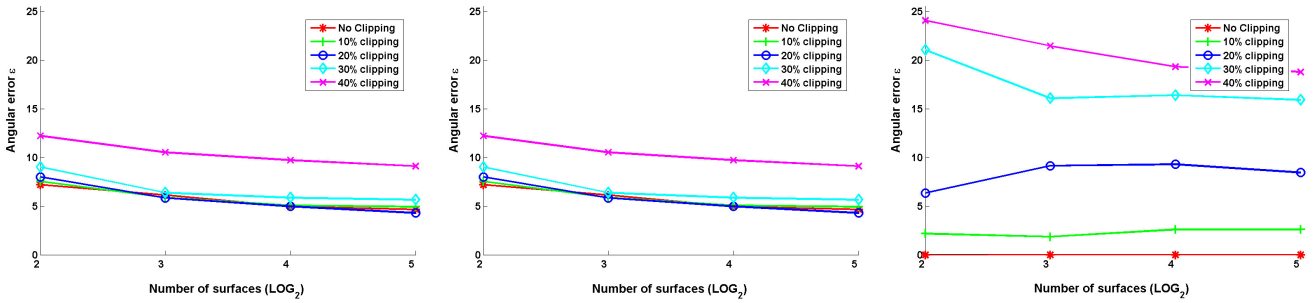

(a) Material edges (b) Shadow edges (c) Specular edges

Figure 3. Mean angular error using material edges, shadow edges and specular edges, for different clipping values.

5.1. Weighting schemes

The experiments of the previous section on a controlled data set are extended to a real-world data set. The real-world data set that is used for this experiment consists of 15 clips with a total of $11,346$ images and is widely used for evaluation of color constancy algorithms. For all images, the ground truth is known from a grey sphere that was mounted on top of the camera, and this sphere was masked during the experiments.

First, several weighting schemes are proposed, based on the photometric edge types discussed in section 3. Using these quasi-invariants, an edge is classified as shadow edge if there is more energy in the shadow-shading variant $\mathbf{S}_x$ than in the specular variant $\mathbf{O}_x$. However, since the shadow-shading variant $\mathbf{S}_x$ measures the amount of energy that is directed towards the shadow-shading direction, this variant can also be used directly to assign higher weights to shadow edges. If all derivative-energy is in the shadow-shading direction, then this indicates that there is a high probability that the current edge is in fact a shadow edge. On the other hand, if no energy is in this direction, then the current edge is likely to be a different type of edge. Hence, the ratio of the energy in the shadow-shading direction versus the total amount of energy can directly be used as a weighting scheme to weight shadow edges more than other types of edges:

$$w_{s,\text{shadow}}(\mathbf{f_x}) = \frac{|\mathbf{S}_x|}{|\mathbf{f_x}|}, \tag{20}$$

where $\mathbf{S}_x$ is the shadow-shading variant.

Using the shadow-shading *in*variant would result in higher weights for specular and material edges, and consequently lower weights for shadow edges:

$$w_{s,\text{spec.+mat.}}(\mathbf{f_x}) = \frac{|\mathbf{S}_x^c|}{|\mathbf{f_x}|}, \tag{21}$$

where $\mathbf{S}_x^c$ is the shadow-shading invariant.

Instead of using the shadow-shading variant and quasi-invariant, the other variants and quasi-invariants can be used. For instance, if the specular variant is used, then specular edges are assigned higher weights. By using the specular quasi-invariant more emphasis is put on the shadow and material edges:

$$w_{s,\text{specular}}(\mathbf{f_x}) = \frac{|\mathbf{O}_x|}{|\mathbf{f_x}|} \tag{22}$$

$$w_{s,\text{shad.+mat.}}(\mathbf{f_x}) = \frac{|\mathbf{O}_x^c|}{|\mathbf{f_x}|}, \tag{23}$$

where $\mathbf{O}_x$ and $\mathbf{O}_x^c$ are the specular variant and quasi-invariant, respectively. The material edges can be emphasized by using the shadow-shading-specular variant and invariant:

$$w_{s,\text{shad.+spec.}}(\mathbf{f_x}) = \frac{|\mathbf{H}_x|}{|\mathbf{f_x}|} \tag{24}$$

$$w_{s,\text{material}}(\mathbf{f_x}) = \frac{|\mathbf{H}_x^c|}{|\mathbf{f_x}|}, \tag{25}$$

where $\mathbf{H}_x$ and $\mathbf{H}_x^c$ are the shadow-shading-specular variant and quasi-invariant, respectively.

Results. The proposed soft weighting schemes are evaluated on the complete set of $11,346$ real-world images [8]. Results of the different soft weighting schemes, using $\kappa = 1$, are shown in table 1(a). Differences between using shadow-shading weighting scheme $w_{s,\text{shadow}}$ or the specular weighting scheme $w_{s,\text{specular}}$ are small. However, assigning higher weights to material edges (i.e. using $w_{s,\text{material}}$) results in a considerably worse performance.

Influence of κ. Using the weighting schemes with a value of $\kappa = 1$ already shows that shadow edges are more valuable than material edges. However, by increasing the value of κ, more weight is assigned to certain edges, effectively enforcing the differences between high and low weights. The effects of κ on the different weighting schemes are shown in figure 4. It can be observed that the shadow-shading weighting scheme benefits, while the performance of the other weighting schemes degrades. An optimal performance is obtained for $\kappa = 10$, resulting in a median angular error of $4.2°$.

Weighting scheme	Median ϵ	
$w_{s,\text{shadow}}$	4.5°	-2%
$w_{s,\text{shadow}}, \kappa = 10$	$\mathbf{4.2}^\circ$	-9%
$w_{s,\text{spec.+mat.}}$	5.8°	$+26\%$
$w_{s,\text{specular}}$	4.4°	-4%
$w_{s,\text{shad.+mat.}}$	5.3°	$+15\%$
$w_{s,\text{material}}$	5.4°	$+17\%$
$w_{s,\text{shad.+spec.}}$	4.5°	-2%

(a) Several soft weighting schemes

Method	Median ϵ
Grey-World	7.0°
White-Patch	5.3°
Shades-of-Grey	5.3°
Grey-Edge	$\mathbf{4.6}^\circ$
2^{nd}-order Grey-Edge	4.9°
Gamut mapping	4.8°

(b) Comparison to state-of-the-art

Table 1. Median angular errors on the real-world set containing 1128 images, using several soft weighting schemes in table (a). The relative performance is with respect to the regular Grey-Edge. In the different weighting schemes, $\kappa = 1$ is used unless stated otherwise. A comparison to state-of-the-art methods is shown in table (b). The soft weighting scheme using the shadow-shading variant $w_{s,\text{shadow}}$ with $\kappa = 10$ outperforms all methods on this set.

5.2. Discussion

The analysis of the influence of κ on the performance of the different weighting schemes corresponds to the findings of section 4, where it is shown that shadow edges are more valuable to estimate the illuminant. Intuitively, a higher value of κ indicates that edges with a high amount of energy in one specific direction are boosted with respect to edges with a medium or low amount of energy in that direction. Hence, in figure 4, it can be observed that boosting the edges with a high amount of energy in the shadow-shading direction is beneficial, while boosting the edges with a high amount of energy in the specular or material direction merely degrades performance. The intuition behind these results is the fact that shadow edges in general are less saturated. Low saturated edges are more affected by the color of the light source than highly saturated edges, so shadow edges relatively contain more information about the color of the light source than non-shadow edges.

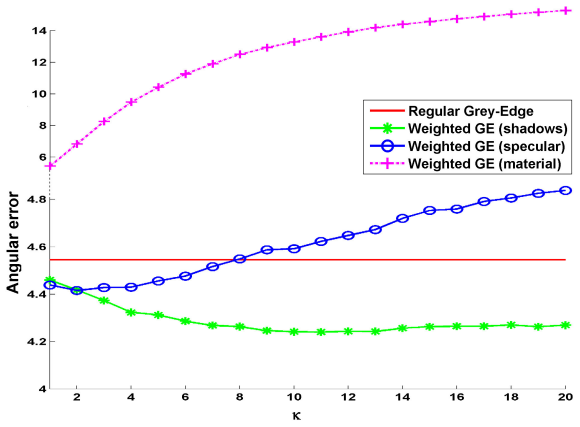

Figure 4. Median angular error of the weighted Grey-Edge using different values for the power κ. Note the change in scale on the y-axis for errors higher than 5, because of the large difference in range of error when using the weights based on material edges.

Compared to current state-of-the-art, the weighted Grey-Edge based on the shadow-shading variant $w_{s,\text{shadow}}$ (using $\kappa = 10$) performs better than all other methods, see table 1. The best-performing pixel-based method is the Grey-Edge ($e_{1,1,1}$) with a median angular error of 4.6°. Note that for the gamut mapping algorithm, the same implementation as in [1] is used, with an empirically determined optimal parameter setting for the current data set. The proposed algorithm using the shadow-shading weighting scheme outperforms these methods with a median angular error of 4.2°, which is an improvement of 9%. The Wilcoxon Sign Test [21] has been computed and shows that this difference is significant with a 99% confidence level.

In figure 5, some example results of the proposed method are shown. Notice the reduction in angular error in the scenes where shadows are present.

6. Conclusion

In this paper, an extensive analysis of the influence of different edge types on the performance of edge-based color constancy has been presented. First, it has been shown that shadow edges are more valuable than material edges, both on spectral data and on real-world data. Then, the weighted Grey-Edge algorithm is proposed. It has been shown that using a soft weighting scheme based on the shadow-shading variant, i.e. assigning higher weights to edges with more energy in the shadow-shading direction, resulted in the best performance. All current state-of-the-art methods, including pixel-based methods and edge-based methods, have been significantly outperformed by the proposed weighted Grey-Edge algorithm, resulting in an improvement of 9% over the current best-performing algorithm.

References

[1] K. Barnard, V. Cardei, and B. Funt. A comparison of computational color constancy algorithms; part i. *IEEE TIP*, 11(9):972–984, 2002.

(a) (b) (c) (d) (e)

Figure 5. Some results of color constancy. In figure (a), the original image is shown, and in figure (b) the result of correction with the true, ground truth, illuminant is shown. In figure (c), the result of the proposed weighted Grey-Edge is shown. In figure (d) and (e), the regular Grey-Edge and Grey-World are shown, respectively.

[2] K. Barnard, G. Finlayson, and B. Funt. Color constancy for scenes with varying illumination. *Comp. Vis. Im. Und.*, 65(2):311–321, 1997.

[3] K. Barnard and B. Funt. Color constancy with specular and non-specular surfaces. In *Proc. CIC*, pages 114–119, 1999.

[4] K. Barnard, L. Martin, B. Funt, and A. Coath. A data set for color research. *CRA*, 27(3):147–151, 2002.

[5] G. Buchsbaum. A spatial processor model for object colour perception. *J. Franklin Institute*, 310(1):1–26, 1980.

[6] A. Chakrabarti, K. Hirakawa, and T. Zickler. Color constancy beyod bags of pixels. In *Proc. CVPR*, 2008.

[7] H. Chen, C. Shen, and P. Tsai. Edge-based automatic white balancing with linear illuminant constraint. In *Visual Communications and Image Processing*, 2007.

[8] F. Ciurea and B. Funt. A large image database for color constancy research. In *Proc. CIC*, pages 160–164, 2003.

[9] M. Fairchild. *Color Appearance Models, 2nd Ed.* John Wiley & sons, Chichester, UK, 2005.

[10] G. Finlayson, B. Funt, and K. Barnard. Color constancy under varying illumination. In *Proc. ICCV*, pages 720–725, 1995.

[11] G. Finlayson, S. Hordley, and P. Hubel. Color by correlation: a simple, unifying framework for color constancy. *IEEE TPAMI*, 23(11):1209–1221, 2001.

[12] G. Finlayson, S. Hordley, C. Lu, and M. Drew. On the removal of shadows from images. *IEEE TPAMI*, 28(1):59–68, 2006.

[13] G. Finlayson, S. Hordley, and I. Tastl. Gamut constrained illuminant estimation. *IJCV*, 67(1):93–109, 2006.

[14] G. Finlayson and E. Trezzi. Shades of gray and colour constancy. In *Proc. CIC*, pages 37–41, 2004.

[15] D. Forsyth. A novel algorithm for color constancy. *IJCV*, 5(1):5–36, 1990.

[16] J. Geusebroek, R. van den Boomgaard, A. Smeulders, and H. Geerts. Color invariance. *IEEE TPAMI*, 23(12):1338–1350, 2001.

[17] T. Gevers and A. Smeulders. Pictoseek: combining color and shape invariant features for image retrieval. *IEEE TIP*, 9(1):102–119, 2000.

[18] T. Gevers and H. Stokman. Classifying color edges in video into shadow-geometry, highlight, or material transitions. *IEEE T. Multimedia*, 5:237–243, 2003.

[19] A. Gijsenij, T. Gevers, and J. van de Weijer. Generalized gamut mapping using image derivative structures for color constancy. *IJCV*, 2009.

[20] S. Hordley. Scene illuminant estimation: past, present, and future. *CRA*, 31(4):303–314, 2006.

[21] S. Hordley and G. Finlayson. Reevaluation of color constancy algorithm performance. *J. Opt. Soc. Am. A*, 23(5):1008–1020, 2006.

[22] E. Land. The retinex theory of color vision. *Scientific American*, 237(6):108–128, December 1977.

[23] J. van de Weijer, T. Gevers, and J. Geusebroek. Edge and corner detection by photometric quasi-invariants. *IEEE TPAMI*, 27(4):625–630, 2005.

[24] J. van de Weijer, T. Gevers, and A. Gijsenij. Edge-based color constancy. *IEEE TIP*, 16(9):2207–2214, 2007.

[25] W. Xiong, B. Funt, L. Shi, S. Kim, B. Kang, and S. Lee. Automatic white balancing via gray surface identification. In *Proc. CIC*, pages 143–146, 2007.